Single-molecule nonequilibrium periodic Mg^{2+}-concentration jump experiments reveal details of the early folding pathways of a large RNA

Xiaohui Qu[†‡], Glenna J. Smith[‡§], Kang Taek Lee[‡§], Tobin R. Sosnick[‡¶], Tao Pan[¶], and Norbert F. Scherer[‡§‖]

Departments of [†]Physics, [§]Chemistry, and [¶]Biochemistry and Molecular Biology, and [‡]Institute for Biophysical Dynamics, University of Chicago, Chicago, IL 60637

Communicated by Paul F. Barbara, University of Texas, Austin, TX, February 14, 2008 (received for review May 21, 2007)

The evolution of RNA conformation with Mg^{2+} concentration ($[Mg^{2+}]$) is typically determined from equilibrium titration measurements or nonequilibrium single $[Mg^{2+}]$-jump measurements. We study the folding of single RNA molecules in response to a series of periodic $[Mg^{2+}]$ jumps. The 260-residue catalytic domain of RNase P RNA from *Bacillus stearothermophilus* is immobilized in a microfluidic flow chamber, and the RNA conformational changes are probed by fluorescence resonance energy transfer (FRET). The kinetics of population redistribution after a $[Mg^{2+}]$ jump and the observed connectivity of FRET states reveal details of the folding pathway that complement and transcend information from equilibrium or single-jump measurements. FRET trajectories for jumps from $[Mg^{2+}] = 0.01$ to 0.1 mM exhibit two-state behavior whereas jumps from 0.01 mM to 0.4 mM exhibit two-state unfolding but multistate folding behavior. RNA molecules in the low and high FRET states before the $[Mg^{2+}]$ increase are observed to undergo dynamics in two distinct regions of the free energy landscape separated by a high barrier. We describe the RNA structural changes involved in crossing this barrier as a ''hidden'' degree of freedom because the changes do not alter the detected FRET value but do alter the observed dynamics. The associated memory prevents the populations from achieving their equilibrium values at the end of the 5- to 10-sec $[Mg^{2+}]$ interval, thereby creating a nonequilibrium steady-state condition. The capability of interrogating nonequilibrium steady-state RNA conformations and the adjustable period of $[Mg^{2+}]$-jump cycles makes it possible to probe regions of the free energy landscape that are infrequently sampled in equilibrium or single-jump measurements.

buffer jump | cooperativity | memory | FRET | electrostatic relaxation

RNA molecules perform both regulatory and catalytic functions (1). Adopting the proper conformation(s) is crucial for their function. Determining the mechanisms by which RNA searches for and finds the proper tertiary structure (i.e., native state) remains a challenging problem (2). Cations, such as Mg^{2+}, are essential to the RNA folding process; nonspecifically bound cations neutralize the highly charged RNA phosphate backbone while specifically bound cations help form and stabilize tertiary interactions and structures (3, 4). The electrostatic and hydrogen-bond (base pairing) interactions create a free energy landscape that determines both the conformational search process and the dynamics related to function.

Like proteins, the free energy landscape of RNA is believed to be rugged. It has been shown that protein dynamics/kinetics can be power law distributed (5, 6) whereas RNA conformational changes tend to exhibit discrete behavior (7, 8). Spontaneous conformational fluctuations associated with thermal motion are observed in equilibrium measurements. Whereas the region near the minimum of the free energy landscape is primarily sampled in equilibrium measurements, nonequilibrium perturbation or (buffer) concentration-jump experiments might probe a larger region as the molecules move farther from their initial equilibrium conformation(s). The nonequilibrium relaxation to new conformations more directly reveal the pathway(s) that RNA molecules take to the new minimum free energy state.

Ensemble concentration-jump measurements using rapid mixing techniques have been widely applied to study RNA and protein folding (9–14). The population relaxation process is assumed to be well described by the fluctuation-dissipation theorem, which, together with detailed balance, allows determination of the equilibrium rate constants (15). The measured ensemble-averaged kinetics allow constructing (minimal) kinetic schemes to describe folding or unfolding.

Single-molecule fluorescence resonance energy transfer (FRET) measurements of surface immobilized RNA have been a powerful approach for studying equilibrium conformational dynamics of DNA and RNA (7, 14, 16–18). By contrast, only a few single-molecule concentration-jump experiments have been reported for RNA (19–21). In these, a single concentration-jump perturbation was applied to the RNA molecules and the subsequent relaxation behavior was observed. These experiments allowed direct observation of an RNA folding pathway.

Here, we use FRET to observe the structural response of single RNA molecules to periodic Mg^{2+} concentration ($[Mg^{2+}]$) jumps (Fig. 1*A*) to study the folding of the 260-residue catalytic domain of the thermophilic RNase P RNA [termed CthermoL18; for details, see refs. 22 and 23, and supporting information (SI) *Materials and Methods* and Fig. S1]. The kinetic scheme shown in Fig. 1*B* illustrates the experiment: each $[Mg^{2+}]$ jump induces a change of the free energy landscape on which the RNA population subsequently redistributes. Alternating forward and reverse jumps create a cycle (24). When the period of the $[Mg^{2+}]$ jumps is longer than the slowest relaxation process, the periodic $[Mg^{2+}]$-jump measurement gives information equivalent to the single-jump experiment. However, when the $[Mg^{2+}]$-jump period is shorter, the distribution of configurations of the RNA molecules before each $[Mg^{2+}]$ jump will be different compared with the single-jump experiment. Therefore, such nonequilibrium steady-state measurements allow probing regions of the free energy landscape that may otherwise escape detection via poor sampling.

For the experiments reported here, the full $[Mg^{2+}]$-jump period is 20 sec; 10 sec each for the low and high $[Mg^{2+}]$ intervals. For CthermoL18, this period is too short for the system to achieve equilibrium before the next jump. This is observed with striking clarity in the kinetics of relaxation associated with each $[Mg^{2+}]$ interval. The range of $[Mg^{2+}]$ jumps used, from 0.01 mM (i.e., low $[Mg^{2+}]$) to 0.1, 0.4, or 1.0 mM (i.e., high $[Mg^{2+}]$),

Author contributions: X.Q., G.J.S., K.T.L., T.R.S., T.P., and N.F.S. designed research; X.Q. performed research; X.Q. analyzed data; and X.Q., G.J.S., and N.F.S. wrote the paper.

The authors declare no conflict of interest.

‖To whom correspondence should be addressed. E-mail: nfschere@uchicago.edu.

This article contains supporting information online at www.pnas.org/cgi/content/full/0801436105/DCSupplemental.

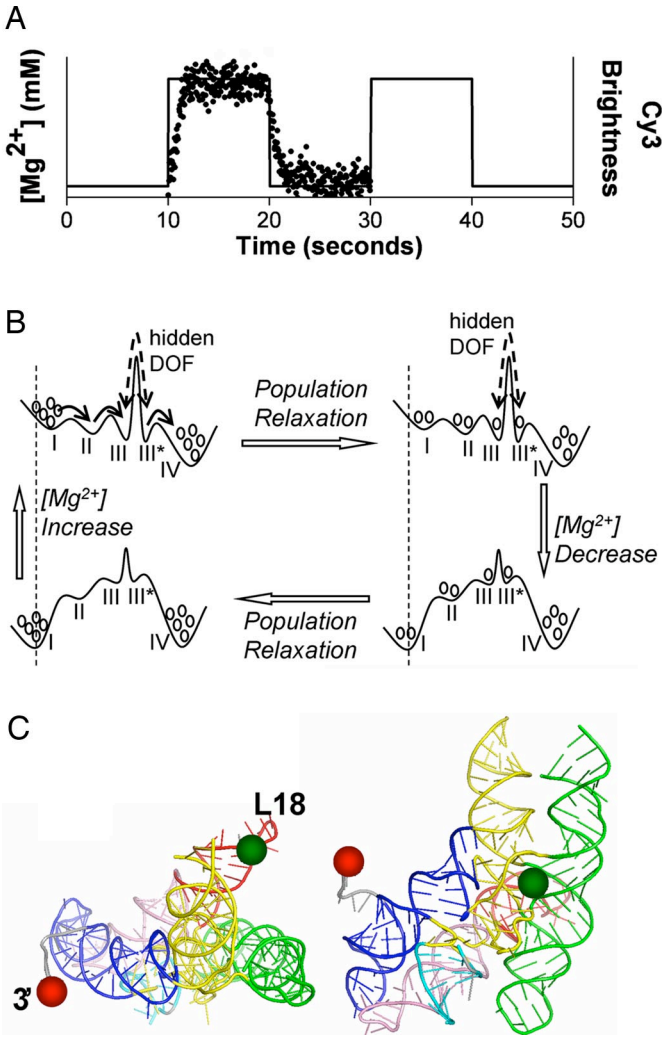

Fig. 1. Schematic of the periodic $[Mg^{2+}]$-jump experiment and cycling of the energy landscape. (*A*) $[Mg^{2+}]$ profile applied in the experiments. The lengths of the high and low $[Mg^{2+}]$ intervals are both 10 sec with a 50 μl/min flow rate for all of the experiments reported here. The solid line shows the idealized $[Mg^{2+}]$ change over time. The overlaid dotted data show the averaged brightness of isolated Cy3 molecules in one field of view. (*B*) Schematic free energy landscape for the periodic $[Mg^{2+}]$-jump experiment. Circles represent the population in each E_{FRET} level. The vertical dashed lines show that the E_{FRET} value of each E_{FRET} state shifts to a higher value at higher $[Mg^{2+}]$ due to electrostatic relaxation. The solid arrows (upper left) represent the folding pathways observed for molecules starting from the low or high E_{FRET} state. These two cases are separated by a high barrier associated with the hidden DOF. The dashed double arrows are meant to indicate that transitions over the high barrier of the hidden DOF are seldom observed within the 10-sec $[Mg^{2+}]$ step. The number of basins, exact barrier heights or well depths, E_{FRET} values, and population at each E_{FRET} state are different for the three $[Mg^{2+}]$-jump conditions. (Note: the coordinates to the left and right of the large barrier are different due to the presence of the state of the hidden DOF. The figure is a 1D representation of a 2D energy landscape.) (*C*) Locations of the L18 loop (Cy3, green spheres) and 3′ end (Cy5, red spheres) on the tertiary structure model of Cthermo from ref. 25.

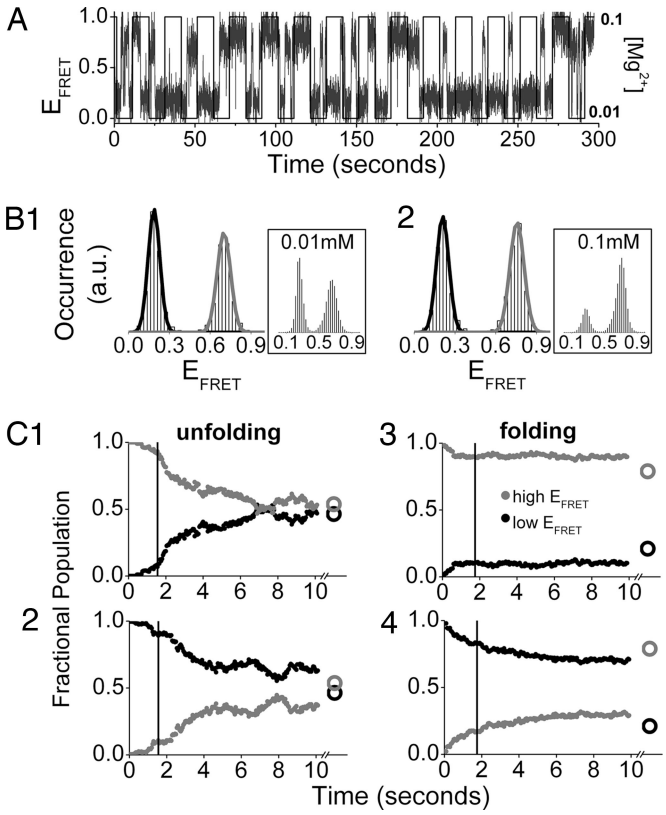

Fig. 2. The 0.01 ↔ 0.1 mM $[Mg^{2+}]$-jump experiment. (*A*) Typical single-molecule trajectory. The $[Mg^{2+}]$ profile (solid square wave) superimposed on the FRET trajectory for a single RNA molecule. (*B*) Cumulative E_{FRET} histograms for folding and unfolding. The histograms are constructed from all of the single-molecule E_{FRET} trajectories in one field of view (≈100 RNA molecules are observed simultaneously). (*Insets*) Equilibrium E_{FRET} histograms. (*C*) Population relaxation kinetics of the low (black) and high (gray) E_{FRET} states. These curves are constructed by sorting all folding and unfolding trajectory segments according to E_{FRET} state before the $[Mg^{2+}]$ jump, and calculating the fraction of molecules that occupy this state at each later time point. The decays are well approximated by exponential fits after the 1- to 2-sec $[Mg^{2+}]$-transition time. (*C1* and *C2*) Unfolding from the high (*C1*) or low (*C2*) E_{FRET} states. (*C3* and *C4*) Folding from the high (*C3*) or low (*C4*) E_{FRET} state. Circles after the split of the time axis show the equilibrium population distributions. Vertical lines at ≈2 sec show when the $[Mg^{2+}]$-transition period ends.

allows probing relatively simple conformational changes (i.e., two-state behavior at 0.1 mM) and complex multistate behavior (at ≥0.4 mM). A general electrostatic response of the RNA structure is immediately observed upon the change in ionic condition. We observe subsequent exponential kinetics in each $[Mg^{2+}]$ interval, but the relaxation at high $[Mg^{2+}]$ is incomplete. Furthermore, by considering the FRET value just before the jump, we identify conformations that are slowly interconverting and therefore separated by a high free energy barrier. The species on either side of this barrier have indistinguishable FRET efficiency (E_{FRET}) values but very different dynamics. Therefore, for single-molecule FRET measurements, the barrier functions as a "hidden" degree of freedom (DOF) that exhibits long memory of the RNA structure and hence influences the individual molecule's dynamics and the kinetics of population relaxation.

Results

Measurements were conducted at three $[Mg^{2+}]$-jump conditions: 0.01 ↔ 0.1, 0.01 ↔ 0.4, and 0.01 ↔ 1.0 mM (see Fig. 1 and *SI Materials and Methods* for details). We refer to the conformational changes of RNA molecules after a $[Mg^{2+}]$ decrease as unfolding, and to those after a $[Mg^{2+}]$ increase as folding. For analysis, trajectories are segmented into unfolding and folding intervals, and these intervals further separated into two cases according to whether the molecule occupied the low or high E_{FRET} state immediately before the $[Mg^{2+}]$ jump (see Fig. 2*C*). The averaged relaxation properties of the resulting four sorted

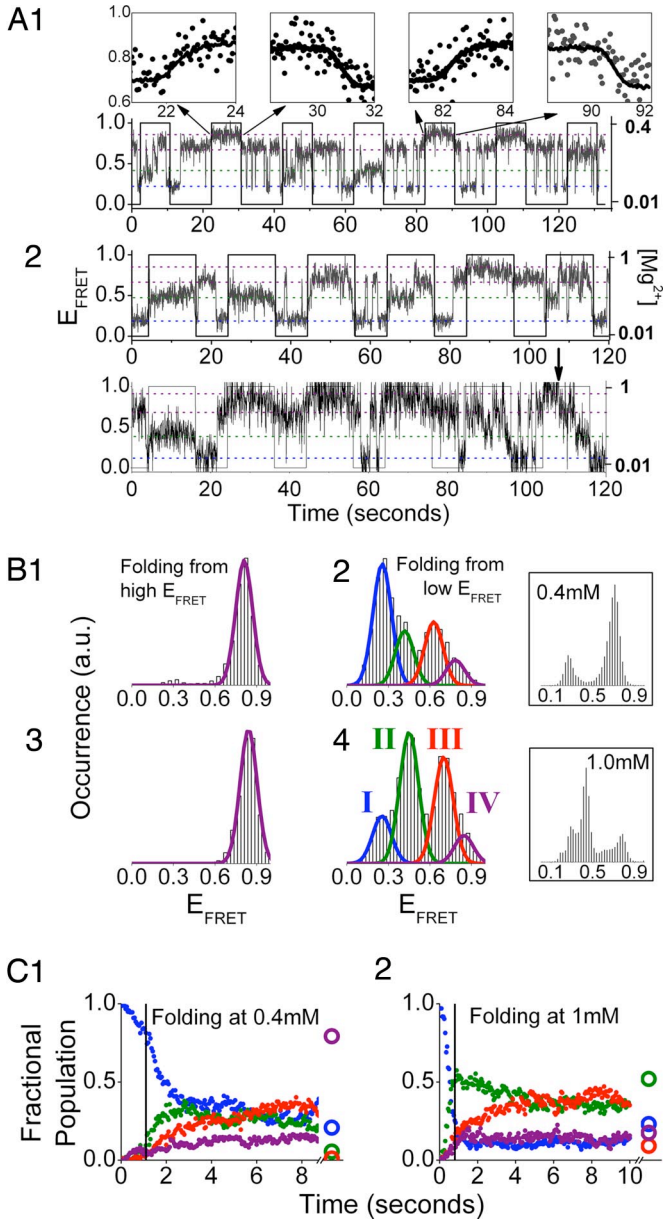

Fig. 3. [Mg^{2+}]-jump experiments for 0.01 ↔ 0.4 mM (*A1*, *B1*, *B2*, and *C1*) and 0.01 ↔ 1.0 mM (*A2*, *B3*, *B4*, and *C2*). (*A*) Representative single-molecule trajectories. (*A1 Insets*) Smooth E_{FRET} change (dots) due to electrostatic relaxation overlap with the measured [Mg^{2+}] profiles (solid lines). The last high [Mg^{2+}] step of the lower trajectory in *A2* shows a rarely observed transition (arrow) over the high barrier associated with the hidden DOF (Fig. 1*B*) whose signature is a transition from the state IV to state III. (*B*) Cumulative E_{FRET} histograms for molecules folding from the high (*B1* and *B3*) and low (*B2* and *B4*) E_{FRET} states. (*Insets*) Equilibrium E_{FRET} histograms. Blue, state I; green, state II; red, state III; purple, state IV (state definition: ref. Table 1). (*C*) Population relaxation kinetics for molecules folding from the low E_{FRET} state. Molecules starting from the high E_{FRET} state only show occasional transitions to state III* and negligible transitions to other E_{FRET} states (data not shown). Two-state behavior similar to that observed in the 0.01 ↔ 0.1 mM experiment (Figs. 2 *B1*, *C1*, and *C2*) is observed at the low [Mg^{2+}] interval for these two jump conditions (data not shown).

sets (unfolding starting low E_{FRET}, unfolding starting high E_{FRET}, folding starting low E_{FRET}, and folding starting high E_{FRET}) are calculated separately and yield key insights into the alternate folding pathways.

We observed two classes of RNA conformational change: (*i*) discrete transitions characteristic of barrier-crossing events that

Table 1. E_{FRET} values at the peak positions of the E_{FRET} histograms in Figs. 2*B* and 3*B*

[Mg^{2+}], mM	E_{FRET} value			
0.01	0.19			0.7
0.1	0.21			0.76
0.4	0.25	0.41	0.62	0.8
1	0.25	0.45	0.7	0.85
(State)	(I)	(II)	(III)	(IV)

Error: ± 0.02 (upper bound). The E_{FRET} states are separated into four groups (I–IV) according to their structural relation by electrostatic relaxation.

are observed during each constant [Mg^{2+}] interval and (*ii*) smooth transitions only observed during the 1-sec [Mg^{2+}]-transition time (see Fig. S2). The smooth transitions track the [Mg^{2+}] change (Fig. 3*A1 Inset*) in a manner consistent with electrostatic relaxation (i.e., collapse or expansion) of RNA structure due to a change in the ionic condition.

Two-State Unfolding and Folding for [Mg^{2+}] = 0.01 ↔ 0.1 mM. E_{FRET} trajectories (Fig. 2*A*; also see Fig. S3) and cumulative E_{FRET} histograms (Fig. 2*B*) show that the RNA exhibits single-transition, two-state behavior for both unfolding and folding in the 0.01 ↔ 0.1 mM experiment. Two-state behavior is consistent with the expectation from our equilibrium study (Fig. 2 *Insets*) (22). The high E_{FRET} peak is more dominant in the folding interval (Fig. 2*B2*) than in the unfolding interval (Fig. 2*B1*), although it is apparent from the peak amplitudes that the population has not yet achieved equilibrium (Fig. 2*B2 Inset*).

The kinetics of population relaxation are clearly different depending on the initial E_{FRET} state immediately before the [Mg^{2+}] jumps, and this difference is especially apparent in the folding interval. If an RNA begins its folding interval from a high E_{FRET} state (Fig. 2*C3*), it tends to stay in the high E_{FRET} state with a population relaxation time constant much longer than the 10-sec jump interval. RNA folding from the low E_{FRET} state (Fig. 2*C4*), in contrast, exhibits relatively fast relaxation. The long-lived high E_{FRET} state observed in the first case is obviously a different conformation than the actively fluctuating high E_{FRET} state visited in the second case. These two high E_{FRET} conformations, distinguished only by their kinetics, reveal a property that we call the "hidden" DOF in CthermoL18. Sensitivity of the relaxation rate and pathways on initial state was observed in previous single-jump studies (19–21).

RNA Conformational Change: Electrostatic Relaxation vs. Barrier-Crossing Process. Electrostatic compaction into a nonspecifically collapsed structure has been shown by time-resolved SAXS to occur in <100 msec (13). When E_{FRET} states at low and high [Mg^{2+}] are grouped together according to their electrostatic relaxation connectivity (Table 1), the E_{FRET} values in each group show a monotonic increase with [Mg^{2+}]. This is consistent with a progressively more collapsed RNA structure at higher [Mg^{2+}] due to better electrostatic screening of the RNA phosphate backbone. This E_{FRET} shift with [Mg^{2+}] is also observed in the E_{FRET} histograms of the equilibrium FRET measurements of the same RNA (22), although in that case the relationship between E_{FRET} states cannot be directly observed.

For the [Mg^{2+}] intervals with only two E_{FRET} states populated, the E_{FRET} states are referred to as low and high. For simplicity, in the case of [Mg^{2+}] intervals with multiple E_{FRET} states, we use group numbers (I–IV) instead of the specific E_{FRET} values (see Table 1 and Fig. 4). The transitions between E_{FRET} states from different groups (see Table 1 and Fig. 4) are barrier-crossing processes that occur during the constant [Mg^{2+}] intervals whereas the transitions between E_{FRET} states within the same

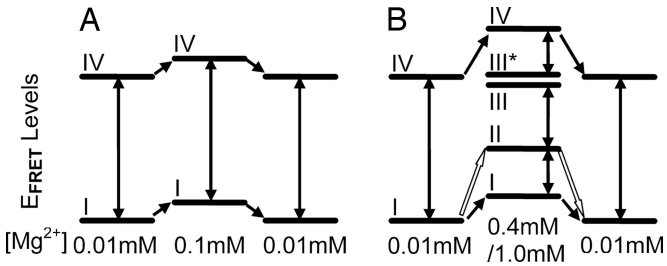

Fig. 4. Connectivity between E_{FRET} states for the three $[Mg^{2+}]$-jump conditions. (*A*) $[Mg^{2+}] = 0.01 \leftrightarrow 0.1$ mM. (*B*) $[Mg^{2+}] = 0.01 \leftrightarrow 0.4$ mM/1.0 mM. The solid double-headed arrows represent RNA conformational fluctuations that happen during the constant $[Mg^{2+}]$ interval and involve barrier crossing with time constants on the order of seconds. The solid single-headed arrows represent electrostatic relaxation of the RNA structure, which follows the $[Mg^{2+}]$-transition curve. In *B*, for the $[Mg^{2+}] = 0.01 \leftrightarrow 1.0$ mM condition, the barrier crossing between state I and state II also happens during the $[Mg^{2+}]$-transition time, simultaneously with the electrostatic relaxation. This is different from other barrier crossing processes (shown as solid double-headed arrows) and thus is represented by open single-headed arrows. States III and III* in *B* have indistinguishable E_{FRET} values within experimental error but differ in dynamic behavior because of difference in hidden DOF. The transitions between III and III* are very rarely observed and thus not represented by arrows. For E_{FRET} states that are not connected by single-headed arrows at $[Mg^{2+}]$ jump, direct transitions between them during $[Mg^{2+}]$-transition time are rarely observed in experiments.

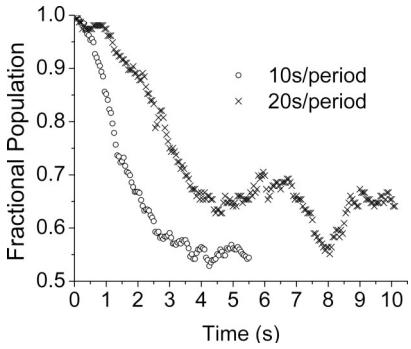

Fig. 5. Relaxation kinetics depend on period length. Shown are the fractional population of the low E_{FRET} state for molecules that are unfolding from the low E_{FRET} state in a $0.01 \leftrightarrow 0.1$ mM jump experiment with either 10-sec (○) or 20-sec (×) periods.

group are electrostatic relaxation processes observed only during the ≈1-sec $[Mg^{2+}]$-transition time. An exception is the conformational change between states I and II for the $[Mg^{2+}] = 0.01 \leftrightarrow 1.0$ mM jump condition, which happens both during the constant $[Mg^{2+}]$ interval (i.e., barrier crossing) and during the $[Mg^{2+}]$-transition time (i.e., barrier crossing happening concurrently with the electrostatic relaxation).

Two-State Unfolding and Multistate Folding for $[Mg^{2+}] = 0.01 \leftrightarrow 0.4$ and $0.01 \leftrightarrow 1.0$ mM. The single-molecule trajectories of Fig. 3*A* show that the $0.01 \leftrightarrow 0.4$ and $0.01 \leftrightarrow 1.0$ mM jump experiments exhibit two-state unfolding. E_{FRET} histograms and population relaxation kinetics are very similar to those of the unfolding interval for $0.01 \leftrightarrow 0.1$ mM just described and thus are not shown, for brevity. In contrast, both jump conditions exhibit complicated multistate folding (Fig. 3). Multistate folding is unexpected for the $0.01 \leftrightarrow 0.4$ mM jump experiment because equilibrium measurements for $[Mg^{2+}] \leq 0.4$ mM (22) show only two-state trajectories for the majority of single molecules. This dramatic deviation from equilibrium behavior is a first indication that the periodic-jump technique is able to probe regions of the free energy surface that are virtually unsampled at equilibrium.

E_{FRET} histograms (Fig. 3 *B1* and *B3*) and trajectories show that RNA molecules folding from the high E_{FRET} state (IV) always go to the highest E_{FRET} state (state IV) with only very infrequent transitions to state III* (Fig. 4). In contrast, molecules folding from the low E_{FRET} state (I) evolve to populate four E_{FRET} states (Fig. 3 *B2* and *B4*), some of which are "intermediate states" not observed in equilibrium measurements (Fig. 3*B Insets*). The folding kinetics for the two-jump conditions will be discussed separately below.

During the $[Mg^{2+}] = 0.4$ mM folding interval (Fig. 3*C1*), RNA molecules that fold from state I primarily go to state II within 3 sec, and the subsequent population relaxation is predominantly to state III. There is also a slow but steady increase in the population of state IV within the 10-sec interval consistent with the expectation from our equilibrium measurements (Fig. 3*B2 Inset*). States II and III are thus intermediates along the folding pathway with state II preceding state III. Because the populations of E_{FRET} states II and III decrease with increasing period of the perturbation (data not shown), one should also consider that these intermediates are sampling conformations in what would be the transition state region at equilibrium.

Folding under the $0.01 \leftrightarrow 1.0$ mM jump condition (Fig. 3*C2*) is similar, and molecules initially in state I again strongly favor going to state II. The transition is fast, complete within the ≈1-sec $[Mg^{2+}]$-transition time. The RNA molecules in state II fold to state III, which continues to accumulate within the 10-sec interval. The difference between folding at 0.4 mM and folding at 1 mM is that the native state is thermodynamically stable and populated at equilibrium at 1 mM. The native state is characterized by an E_{FRET} value of 0.45 (22), indistinguishable from the E_{FRET} value of state II (Fig. 3*B4 Inset*), suggesting similarity in conformation (or distance between dye molecules) for these two states as probed by FRET. However, the population of state II does not increase monotonically in the folding interval, as would be expected for the native state (see ref. 22). This contradiction is strong evidence that state II is not identical to the native state, and that these two states differ in some hidden DOF. We conclude that the observed axis responds rapidly to the $[Mg^{2+}]$ change while equilibration of the hidden DOF is slower. A much longer time ($\gg$10 sec) is required for both the observed axis and the hidden DOF to relax to the native state.

Variation of $[Mg^{2+}]$ Period. To further establish the sensitivity to hidden DOFs and non-Markovian dynamics, we varied the period of the perturbation. Fig. 5 shows a comparison of the low E_{FRET}, low $[Mg^{2+}]$ subensemble results for 20- and 10-sec periods (i.e., 10- and 5-sec intervals at the high and low $[Mg^{2+}]$ condition). If the dynamics were a two-state (Markovian) process, one would expect the relaxation rates to be the same. However, the shorter-period data relax much faster. In comparison to the shorter high $[Mg^{2+}]$ interval, the RNA molecules are driven further from the low $[Mg^{2+}]$ steady-state (almost equilibrium) position in the longer high $[Mg^{2+}]$ interval. Because the observed DOF then has more time to "couple" with the hidden DOF, the dynamics of the observed DOF become slower (or more non-Markovian). In the language of this article, the more time the molecules are allowed to fold during the high $[Mg^{2+}]$ interval, the more the single molecules change their conformations along the hidden DOF(s), and hence the slower the unfolding during the low $[Mg^{2+}]$ interval.

Discussion

Folding at High $[Mg^{2+}]$ Is Slow and Multistate Whereas Unfolding at Low $[Mg^{2+}]$ Is Fast and Two-State. For the unfolding interval, all three jump experiments exhibit two-state kinetics, and the population distributions at the end of the 10-sec interval are close to the equilibrium result (Fig. 2 *C1* and *C2*; unfolding intervals for the $0.01 \leftrightarrow 0.4$ and $0.01 \leftrightarrow 1$ mM $[Mg^{2+}]$ are not

shown for brevity). This population shift indicates that at low $[Mg^{2+}]$, relaxation appears to be nearly complete within the 10-sec interval regardless of the initial E_{FRET} state or original high $[Mg^{2+}]$. Folding, however, is more complicated; multiple intermediate states are involved and events originating from the low or high E_{FRET} states behave very differently. Unfolding involves spontaneous opening of the RNA structure, while folding is entropically unfavorable, requiring structural elements to assemble in the correct order. The E_{FRET} population distributions at the end of the high $[Mg^{2+}]$ interval for all three jump conditions (Figs. 2 *C3* and *C4* and 3*C*) are far from their equilibrium distributions. Thus, the RNA population does not achieve equilibrium in the 10-sec high $[Mg^{2+}]$ interval. This is consistent with previous observations that folding is slower and more complex than unfolding (21).

Hidden Degrees of Freedom and Long Memory Effect. The crystal structure of RNase P RNA (25) suggests that the positions labeled with the FRET dyes (3′ end and L18 loop) are not directly involved in the formation of the core structure. However, it is reasonable to expect that the observed (i.e., labeled) DOF can report on the structure and dynamics of the unlabeled parts of the RNA due to structural connectivity (22). All three jump experiments reported here indicate that the structural changes of the unlabeled parts of the RNA molecule affect the observed dynamics of the labeled axis but not the E_{FRET} values. Folding at $[Mg^{2+}] = 0.1$ mM is characterized by two kinetically distinct high E_{FRET} states: molecules that fold from an initial high E_{FRET} state end up in a stable long-lived high E_{FRET} state whereas molecules that fold from the low E_{FRET} state fluctuate quite actively between low and high E_{FRET} states. These two behaviors result from conformational differences in the hidden DOFs. Folding at $[Mg^{2+}] = 1$ mM includes transient population of a E_{FRET} state (state II) with the same E_{FRET} value as the native state, although it behaves as a kinetic intermediate. Further structural changes in a hidden DOF require much longer than 10 sec to attain the native state.

Slow dynamics in the hidden DOFs give rise to long memory effects in the single-molecule E_{FRET} trajectories. Fig. S4 shows RNA molecules that retain dramatically different dynamics in the observed FRET DOF for several minutes; some molecules remain in the low or high E_{FRET} states (Figs. S4 *a* and *b*) whereas other molecules synchronize with the periodic $[Mg^{2+}]$ jumps and switch between low and high E_{FRET} states (Fig. S4*c*). Persistent behavior is likely to result from structural/conformational differences in some hidden DOF.

Stabilizing Effects of Mg^{2+} on RNA Structure and Cooperative RNA Folding. Mg^{2+} ions stabilize RNA structure by allowing tertiary contacts to form through specific ion binding, and by electrostatically screening the phosphate backbone (3). For all three jump conditions, the RNA molecules were observed to become compact upon an increase in $[Mg^{2+}]$ (Fig. 4). This compaction is likely due to the nonspecific electrostatic relaxation of the RNA structure, but it has been shown for other RNA molecules that some tertiary interactions might also be formed during the electrostatic relaxation process (4, 26). Achieving high cooperativity in folding (27, 28) requires some preorganization of the structure. We believe that topological constraints of the native state require formation of the following helices: P4 first, then P2, then finally P5, with a number of noncanonical stabilizing interactions (22). Formation of these helices in different order or combinations may result in intermediate states that are kinetically stable.

No ensemble kinetic experiments have been reported for the Cthermo thermophilic ribozyme. However, a rate-limiting step along the folding pathway of a mesophilic homologue has been characterized in ensemble measurements. A folding (29) and unfolding (30) intermediate was directly observed and deduced from a $[Mg^{2+}]$-chevron analysis (12). The rate-limiting step to the native state was described as a small-amplitude conformational change (i.e., no change in radius of gyration or burial of surface area) between these two intermediate states (29). No additional Mg^{2+} ions are bound in this step, which argues for a local consolidation of RNA structure around a prebound Mg^{2+} ion. This lack of change in global structural dimensions is consistent with the indistinguishable E_{FRET} values of states III and III* and would suggest that these states lie on either side of the major barrier (Fig. 1*B*).

In the mesophilic homologue, the folding rate at high $[Mg^{2+}]$ is more than one order of magnitude slower than the unfolding rate at very low cation concentration (29). This difference is qualitatively consistent with our observation that for all three jump conditions, unfolding is largely complete within the 10-sec low $[Mg^{2+}]$ interval whereas folding is far from equilibrium within the 10-sec high $[Mg^{2+}]$ interval (Figs. 2*C* and 3*C*). Thus, our observation that the folding barrier is higher under folding conditions compared with the unfolding barrier under unfolding conditions in the $[Mg^{2+}]$ jump experiments of CthermoL18 RNA agrees with the ensemble kinetic measurements of the mesophilic homologue.

Free Energy Landscape. The connectivity of the E_{FRET} states along the folding pathway (Figs. 2*C*, 3*C*, and 4) and the rate constants for interconversion between two connected E_{FRET} states (Table S1) are readily obtained from the single-molecule RNA response to $[Mg^{2+}]$ jumps monitored over time. Although each jump experiment differs in detail (e.g., the barrier heights and number of free energy basins), a qualitative free energy landscape with the major features of all three jump experiments can be illustrated as in Fig. 1*B*. A $[Mg^{2+}]$ change causes the free energy landscape to shift with subsequent RNA population redistribution toward equilibrium on the new free energy landscape. Molecules traverse different regions of the landscape depending on which E_{FRET} state [low (I) or high (IV)] a molecule occupies before the $[Mg^{2+}]$ jump. The two regions are separated by a high barrier that corresponds to a structural change in some hidden DOF. During folding, this barrier is so high that transitions over it are only rarely observed. For the $0.01 \leftrightarrow 0.4$ mM and $0.01 \leftrightarrow 1.0$ mM jump conditions, the E_{FRET} histograms (Fig. 3*B*), connectivity of the E_{FRET} states (Fig. 4), and (rare) observation of transitions over the barrier (Fig. 3*A2*, lower trajectory, arrow) allow assignment of the barrier between states III and III*—they possess the same observed E_{FRET} value but are kinetically distinct and therefore on opposite sides of the barrier.

Probing Regions of the Free Energy Landscape That Are Inaccessible to Equilibrium Results. In contrast to perturbation experiments with only a single jump, the period of the periodic-jump experiment can be used to probe macromolecular free energy landscapes. When the period of $[Mg^{2+}]$ jumps is shorter than the time scale for relaxation, the distribution of RNA conformations at the end of an interval will not have reached equilibrium. The response of this nonequilibrium distribution of starting conformations to the next $[Mg^{2+}]$ jump will depend on how far the system is from each of the two asymptotic equilibrium distributions. The system's "distance" from equilibrium is controlled by the length of the periodic $[Mg^{2+}]$ jumps. Fig. 5 shows that the ribozyme is perturbed less during the 5-sec interval (vs. 10-sec interval), and so it relaxes more quickly. If one assumes linear response (but near equilibrium), then the relaxation rate should be independent of perturbation. The observed dependence of relaxation kinetics on the length of the $[Mg^{2+}]$-jump period is evidence that a nonlinear (or non-Markovian) response describes the RNA dynamics in this experiment. Additionally, the RNA populations driven for different periods cannot be equilibrating to the same distributions of states. Therefore, different

regions of the free energy surface are probed with different period lengths. The result of the period dependence is a direct manifestation of memory in the dynamics. With a long enough sequence of periodic-jump cycles, the molecules are best described by a nonequilibrium steady-state distribution of conformations (31). Because the effective steady-state landscape is different from either equilibrium limit, one can picture that the set of conformations sampled may be those close to the transition state separating the basins (note state II in Fig. 3*C1*).

Conclusions

We developed and applied a single-molecule periodic $[Mg^{2+}]$-jump method to study the Mg^{2+}-induced folding of CthermoL18 RNA. The observed connectivity of E_{FRET} states and the associated rate constants allow construction of new details of the free energy landscape. We find that molecules starting from the two different interconverting conformations (i.e., the low and high E_{FRET} states) before a $[Mg^{2+}]$ increase traverse two distinct regions of the landscape, which are separated by a very high free energy barrier. This rate-limiting step involves only changes in the hidden DOF and does not induce detectable change in the E_{FRET} value. The slow dynamics, apparent in the hidden DOF, give rise to more details of the free energy landscape and clearly reveal long memory effects in the single-molecule E_{FRET} trajectories. The fact that the relaxation dynamics depend on the magnitude (duration) of the perturbation for a fixed $[Mg^{2+}]$ clearly indicates that the response is non-Markovian as is expected for a nonequilibrium steady-state system with long memory.

Many important RNA folding questions can be studied with this approach, such as the origin and properties of long memory effects, and cooperative folding of large RNAs at high $[Mg^{2+}]$. Quantitative modeling of the observed dynamics, such as a generalized Langevin equation simulation with a memory kernel (32), will provide more insights into RNA folding mechanisms. Finally, measurements with a set of different $[Mg^{2+}]$-jump periods will allow construction of a more comprehensive free energy landscape that is inaccessible from equilibrium measurements and traditional single-jump techniques.

Materials and Methods

The experimental methods are briefly described here and in detail in *SI Materials and Methods*. A microfluidic channel ≈800-μm-wide with two short input branches in a ''Y''-shape was cut into an adhesive spacer (Grace Biolabs). The flow chamber was completed by coupling the spacer to a polyethylene glycol (PEG)-coated coverslip and to a glass slide. Holes were drilled through the glass slide to allow connection of the two input channels of the flow chamber via polyethylene tubing to individual syringes filled with buffers of the desired $[Mg^{2+}]$. Two computer-controlled PHD2000 syringe pumps (Harvard Apparatus) were used to achieve the desired flow profile (see Fig. 1*A*).

RNA molecules labeled with the FRET dye pair and biotin were attached to Streptavidin molecules that have been immobilized to the coverslip. The FRET measurement was conducted on a home-built objective-type total internal reflection fluorescence (TIRF) microscope, using an EM-CCD detector (Andor Technology). Time trajectories of donor and acceptor molecules were extracted from the images for each RNA molecule by using a routine written in MATLAB (MathWorks).

ACKNOWLEDGMENTS. We thank the Ismagilov group, especially Helen Song, for help with making PDMS devices and discussions about microfluidic systems. This work was supported by National Institutes of Health Grant GM067961 and Burroughs Wellcome Fund Interfaces ID 1001774 through a fellowship to X.Q. N.F.S. thanks the John S. Guggenheim Foundation for a fellowship.

1. Alberts B (2002) *Molecular Biology of the Cell* (Garland Science, New York).
2. Lilley DMJ (2005) Structure, folding and mechanisms of ribozymes. *Curr Opin Struct Biol* 15:313–323.
3. Draper DE, Grilley D, Soto AM (2005) Ions and RNA folding. *Annu Rev Biophys Biomol Struct* 34:221–243.
4. Woodson SA (2005) Metal ions and RNA folding: A highly charged topic with a dynamic future. *Curr Opin Chem Biol* 9:104–109.
5. Iben IET, *et al.* (1989) Glassy behavior of a protein. *Phys Rev Lett* 62:1916–1919.
6. Min W, Luo GB, Cherayil BJ, Kou SC, Xie XS (2005) Observation of a power-law memory kernel for fluctuations within a single protein molecule. *Phys Rev Lett* 94:198302.
7. Zhuang XW (2005) Single-molecule RNA science. *Annu Rev Biophys Biomol Struct* 34:399–414.
8. Nahas MK, *et al.* (2004) Observation of internal cleavage and ligation reactions of a ribozyme. *Nat Struct Mol Biol* 11:1107–1113.
9. Eigen M, Hammes GG (1960) Kinetic studies of Adp reactions with the temperature jump method. *J Am Chem Soc* 82:5951–5952.
10. Munoz V, Thompson PA, Hofrichter J, Eaton WA (1997) Folding dynamics and mechanism of β-hairpin formation. *Nature* 390:196–199.
11. Krantz BA, Sosnick TR (2000) Distinguishing between two-state and three-state models for ubiquitin folding. *Biochemistry* 39:11696–11701.
12. Fang XW, Pan T, Sosnick TR (1999) Mg^{2+}-dependent folding of a large ribozyme without kinetic traps. *Nat Struct Biol* 6:1091–1095.
13. Russell R, *et al.* (2002) Rapid compaction during RNA folding. *Proc Natl Acad Sci USA* 99:4266–4271.
14. Downey CD, *et al.* (2006) Metal ion dependence, thermodynamics, and kinetics for intramolecular docking of a GAAA tetraloop and receptor connected by a flexible linker. *Biochemistry* 45:3664–3673.
15. Chandler D (1987) *Introduction to Modern Statistical Mechanics* (Oxford Univ Press, New York).
16. McKinney SA, Freeman ADJ, Lilley DMJ, Ha TJ (2005) Observing spontaneous branch migration of Holliday junctions one step at a time. *Proc Natl Acad Sci USA* 102:5715–5720.
17. Cosa G, *et al.* (2006) Evidence for non-two-state kinetics in the nucleocapsid protein chaperoned opening of DNA hairpins. *J Phys Chem B* 110:2419–2426.
18. Rueda D, *et al.* (2004) Single-molecule enzymology of RNA: Essential functional groups impact catalysis from a distance. *Proc Natl Acad Sci USA* 101:10066–10071.
19. Ha T, *et al.* (1999) Ligand-induced conformational changes observed in single RNA molecules. *Proc Natl Acad Sci USA* 96:9077–9082.
20. Zhuang XW, *et al.* (2000) A single-molecule study of RNA catalysis and folding. *Science* 288:2048–2051.
21. Russell R, *et al.* (2002) Exploring the folding landscape of a structured RNA. *Proc Natl Acad Sci USA* 99:155–160.
22. Smith G, *et al.* (2008) A large collapsed-state RNA can exhibit simple exponential single-molecule dynamics. *J Mol Biol* 378:941–951.
23. Smith GJ, Sosnick TR, Scherer NF, Pan T (2005) Efficient fluorescence labeling of a large RNA through oligonucleotide hybridization. *RNA* 11:234–239.
24. Hill TL, Hill TL (1989) *Free Energy Transduction and Biochemical Cycle Kinetics* (Springer, New York).
25. Kazantsev AV, *et al.* (2005) Crystal structure of a bacterial ribonuclease P RNA. *Proc Natl Acad Sci USA* 102:13392–13397.
26. Kwok LW, *et al.* (2006) Concordant exploration of the kinetics of RNA folding from global and local perspectives. *J Mol Biol* 355:282–293.
27. Fang XW, Srividya N, Golden BL, Sosnick TR, Pan T (2003) Stepwise conversion of a mesophilic to a thermophilic ribozyme. *J Mol Biol* 330:177–183.
28. Fang XW, *et al.* (2001) The thermodynamic origin of the stability of a thermophilic ribozyme. *Proc Natl Acad Sci USA* 98:4355–4360.
29. Fang XW, Thiyagarajan P, Sosnick TR, Pan T (2002) The rate-limiting step in the folding of a large ribozyme without kinetic traps. *Proc Natl Acad Sci USA* 99:8518–8523.
30. Baird NJ, Fang X-W, Srividya N, Pan T, Sosnick TR (2007) Folding of a universal ribozyme: The ribonuclease P RNA. *Q Rev Biophys* 40:113–161.
31. Tietz C, Schuler S, Speck T, Seifert U, Wrachtrup J (2006) Measurement of stochastic entropy production. *Phys Rev Lett* 97:050602.
32. Min W, Xie XS (2006) Kramers model with a power-law friction kernel: Dispersed kinetics and dynamic disorder of biochemical reactions. *Phys Rev E* 73:010902.